

Plasma-catalysis chemical looping CH₄ reforming with water splitting using ceria supported Ni based La-perovskite nano-catalyst

Rajagopalan V. Ranganathan^a, Bodiuzzaman Jony^b, Steven M. Fondriest^a, Zhongqi Liu^c, Ruigang Wang^c, Mruthunjaya Uddi^{a,*}

^a Mechanical Engineering, The University of Alabama, Tuscaloosa, AL, 35487, United States

^b Aerospace Engineering and Mechanics, The University of Alabama, Tuscaloosa, AL, 35487, United States

^c Metallurgical and Materials Engineering, The University of Alabama, Tuscaloosa, AL, 35487, United States

ARTICLE INFO

Keywords:

Chemical looping reforming
Plasma catalysis
Methane reforming
Water splitting

ABSTRACT

Chemical Looping reactions have the advantage of producing useful chemicals, with minimal energy penalty while achieving Carbon Capture Sequestration (CCS). We present the results of Plasma Catalytic (PC) CH₄ reforming reduction step coupled with PC water splitting oxidation step to produce hydrogen. We use CH₄ + CO₂ flow reduction step with nano-powder, 50:50 mass ratio of La_{0.9}Ce_{0.1}NiO₃ perovskite with CeO₂ solid mixture as catalyst with Oxygen Carrier (OC) combination. The material is oxidized with H₂O + Ar during the oxidation step leading to H₂ production by water splitting. The primary goal is to study the plasma-assisted reforming and water splitting, with the purpose of achieving reactions at low temperatures (150–400 °C). Water splitting H₂ production (24–30 μmole/g total) and CH₄ reforming (14–43 % conversion) were observed in the temperature range of 150–400 °C, while no such reactions were observed without plasma in this low temperature range, with just the oxygen carrier nano-materials. Substantial enhancements were also observed at higher temperatures.

1. Introduction

The continuous rise of CO₂ emission and its accumulation in the atmosphere are among the main reasons for global warming. The present atmospheric concentration of CO₂ is already approaching 400 ppm [1]. Therefore, extensive research efforts are under way to decrease CO₂ emission by various means such as Chemical-looping (CL) which is a promising method to achieve Carbon Capture Sequestration (CCS). CL is a novel and promising technology [2,3] for several applications including oxy-combustion for CCS, H₂ production [4], methane reforming [4] and CO₂ reuse [5–9]. One of the primary issues in conventional post-combustion CCS is the energy penalty involved in separating CO₂ from N₂ containing exhaust in the power plants. CL addresses this issue by using an Oxygen Carrier (OC) material (such as metal oxide-Me_xO_y in Fig. 1) and cycling it through periodic oxidation and reduction steps instead of supplying oxygen directly from air. The exhaust gas contains only CO₂ and H₂O. This makes it easy to separate CO₂ for CCS. The energy penalty is lesser than post-combustion separation of CO₂. Chemical Looping Reforming (CLR) with Water Splitting (CLRWS), studied here, enables CO₂ utilization with CH₄ to produce useful products such as CO and H₂, as shown in Fig. 1 during the reduction step, and can produce H₂ by H₂O splitting during the oxidation step.

Hydrogen is generally produced by traditional Steam Methane Reforming (SMR) which involves multiple steps with high capital investment. The components involved are supply of natural gas feedstock, catalyst and steam, pre-reformer, a steam reformer, heat exchanger units, shift reactors, and a pressure swing adsorption unit. Achieving CCS needs additional equipment leading to higher cost of H₂ generation (22% increase) and incomplete CO₂ capture [4,10].

CL has the advantages of achieving CCS with minimal energy penalty and lesser capital investments as discussed by Luo et al. [4] on hydrogen production using CL technology. No external heating is required leading to lesser CO₂ emissions and improved efficiency. Less steam and catalysts are required, there is less concern with respect to sulfur contaminants, and there is no thermal NO_x formation. It can have much higher (by 6% points [11]) effective thermal and carbon capture efficiency compared to SMR. In recent years DOE (Department of Energy-USA) has invested heavily in CL research [12–14].

In CL the reaction process is decomposed into two “redox” steps (Fig. 1) -reduction and oxidation. The redox reactions take place in two separate chambers. During the reduction step, a mixture of CO₂ and CH₄ is flowed over a metal oxide (Me_xO_y) in a fuel reactor to generate CO, H₂, CO₂, and H₂O, reducing the metal oxide (to Me_xO_{y-1}). During the oxidation step, water vapor is flowed over the “reduced” metal

* Corresponding author.

E-mail address: uddi@ua.edu (M. Uddi).

<https://doi.org/10.1016/j.jcou.2019.03.014>

Received 4 December 2018; Received in revised form 5 March 2019; Accepted 18 March 2019

2212-9820/ © 2019 Elsevier Ltd. All rights reserved.

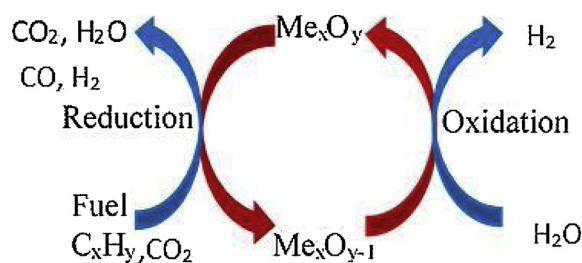


Fig. 1. Chemical Looping Reforming (CLR) process with water splitting (CLRWS). (Color lines are seen in online version only). CLR enables usage of CO₂ for dry reforming with CH₄.

oxide (Me_xO_{y-1}) to reoxidize it while producing pure H₂. The metal oxide (Me_xO_y) acts as an Oxygen Carrier (OC) from the oxidation step to the reduction step. The OC material can be a metal (eg. Fe, Cu, Ni, Co) [15] or their oxides, oxides such as CeO₂ [5] or a perovskite [16]. Our current studies need OC material suitable for both reforming (a catalyst) and water splitting. OCs such as Fe₃O₄, Cu produce mostly complete CH₄ combustion products (CO₂ + H₂O). OCs such as Ni, CeO₂ are known to favor syngas (CO + H₂) production.

One of the most commonly studied OCs for CH₄ reforming is nickel [15,17–22]. Coke formation and agglomeration are primary concerns with Ni-based OC. Expensive noble metals like Pt [23,24] and Ru [25,26] show higher catalytic activity and less coke formation for dry reforming of methane. CeO₂ is known to reduce carbon deposition due to the lattice oxygen ion which helps in oxidizing deposited carbon [27]. However, the catalysts and OC materials are still limited by low reactivity below 850 °C.

Currently, there are several CL reactors used both commercially and on lab test scale (see reviews [3,4]). There have been several studies (e.g [8,28–30]) to implement CL for solar to chemical production. One example is the thermochemical CL [30] where, reduction step involves heating the reactor to high temperatures (1200–1800 °C), while the water splitting oxidation step is at lower temperatures (800–1000 °C). The high reduction step temperatures leads to inefficient use of high quality energy and exergy destruction [31], and there have been efforts [29,30] to reduce the peak operation temperatures.

The reduction in operation temperature with plasma-catalysis has several cost and efficiency advantages in reactor design [32], lower entropy generation, reduced heat losses, reactor lifespan, reduced catalyst deactivation, and lesser water vapor heating requirements etc. It also opens the opportunities for using low cost solar energy reactors, wind energy, and waste heat. We think that the plasma catalysis is particularly suited for small scale applications such as in the case of solar ceria foam reactor [33] or Rotary Bed Reactor [34].

In a variation of thermochemical CL cycle, fuel such as CH₄ can be used to reduce the OC instead of heating it to high temperatures, while producing useful chemicals such as syngas as already explained. In state of the art CL experiments with fuel reduction step, Zhao et al. [3] studied isothermal furnace redox cycles using CeO₂ as OC/catalyst material. Fuel was used for reducing the OC during the reduction step at reactor temperatures in the range of 750–1000 °C. They found two orders of magnitude higher production rate of H₂ (100–300 μmole/g/s) by water splitting in the oxidation step, compared to thermochemical looping [35].

It has been found that CeO₂ produced higher water splitting rates in CL compared to most other materials found in the literature [3]. A review of other materials used for isothermal CL can be found in [3,5]. More recently, Ruan et al. [29] obtained similar water splitting enhancements as Zhao et al. [3] using Ni promoted ceria–titanium oxide (CeO₂–TiO₂) CL material, achieving almost complete CH₄ reforming in the reduction step at 900 °C. However, there have been continued efforts to reduce operation temperatures of the CL cycles. More recently, plasma-catalysis (PC) has been studied to achieve low temperature

operation of CL cycles by taking combined advantages of reaction rate enhancing abilities of both catalysts and non-equilibrium plasma discharge [36], acting synergistically [37–39].

PC has been found to enhance plasma combustion [36,40] and heterogeneous reactions [37,39,41–44] at low temperatures. Whitehead et al. [45], demonstrated the experimental PC synergy in the destruction of toluene, considered as an example of atmospheric pollutant, achieving higher energy efficiency over just catalytic or plasma process. They also found an energy saving of ~34% using the plasma-catalyst combination. Other promising results of PC synergy have been summarized in several reviews [37,39,41–44]. The results show endless possibilities when the radicals, ions, electrons, vibrationally, rotationally and electronically excited species produced in a non-equilibrium low temperature plasma are combined with the advantages of nanocatalysts. More recently, Mehta et al. [37] showed the possible advantages of N₂ vibrational excitation in PC synthesis of NH₃ through DFT calculations.

Non-equilibrium plasma is characterized by large differences between the electron temperature of a plasma (usually > 40,000 K) and the neutral gas temperature, which is usually close to the furnace temperature [46]. The current flow through the non-equilibrium plasma is also much lesser (~mA) compared to equilibrium arc discharges (A), where the electron and neutral/ion temperatures are very close to each other. Therefore, the power requirements of non-equilibrium plasma are much less while abundant concentrations of highly reactive radicals/species are generated by electron impact on molecules.

The goal of this study is to achieve simultaneous CLR (reduction step) and water splitting (oxidation step) at much lower temperatures (150–500 °C), which could enable the development of efficient reactors using renewable energy sources. We adopt PC to achieve the aforementioned goal using nano-powder 50:50 mass ratio of La_{0.9}Ce_{0.1}NiO₃ and CeO₂ solid mixture as catalyst and OC combination. The La_{0.9}Ce_{0.1}NiO₃ has been found to be a very good CH₄ reforming catalyst [47] while CeO₂ is known for high lattice and surface oxygen ion mobility [48,49] leading to faster reaction rates and lesser carbon deposition. CeO₂ also has a very good oxygen carrying capacity (oxygen storage and fast release capacity). Since Ni based perovskite has been demonstrated as a very good reforming catalyst in literature [47], we combined it with ceria which is known to have high Oxygen Storage Capacity (OSC), to take advantages of both materials for the chemical looping reforming (reduction step) coupled with water splitting oxidation step. It is possible that both perovskite and ceria are oxygen carriers in our experiment. Here, for the first time, we present experimental results of PC-CL reactions with water splitting oxidation step coupled with CH₄/CO₂ reforming. We placed the CL material directly in the non-equilibrium plasma and gas flow, to realize maximum PC synergy effects.

Although not much is known, possible surface synergistic plasma-catalysis reaction mechanisms are shown in Fig. 2. Plasma also provides a platform to study radical specific surface chemistry by producing abundant radicals and electronically/vibrationally excited species. The gas phase CH₄ combustion generally proceeds by H abstraction reactions by attack of O, OH, O₂ radicals [50]. The intermediate products of CH₄ combustion include species such as CH_x (x = 1–3), CH₃O, CH₂O, HCO, and COOH. Since plasma can dissociate CH₄, by electron impact, into radicals such as CH_x (x = 1–3) and H and can also dissociate CO₂ to CO and O, the gas phase reactions are enhanced at low temperatures [36,51]. Additionally these plasma generated radicals and vibrationally excited species can readily adsorb [52,53] on the CL material, perovskite-ceria interface and react with lattice oxygen ions. Therefore a complex gas phase coupled heterogeneous reaction chemistry is expected during the reduction step. All surface reaction mechanisms Mars-van Krevelen (MvK), Eley-Rideal (ER) and Langmuir Hinshelwood (LH) mechanisms are expected to be dominant and coupled in a complex manner. Strong Metal Support Interaction (SMSI) [54] between

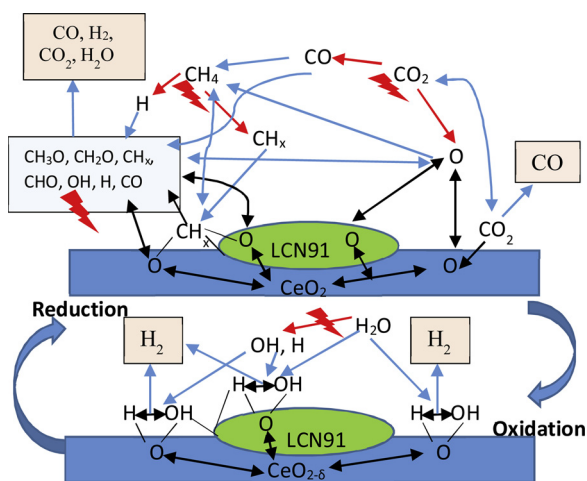


Fig. 2. Schematic of possible plasma-catalysis heterogeneous reaction mechanisms. Red lines show plasma generation of species, blue lines show formation of gas phase and adsorption ready species, black lines show adsorption interaction, surface reactions and oxygen ion diffusion.

ceria support and perovskite can play an important role in the surface chemistry of both reduction and oxidation step, and reduce carbon deposition by reacting with it to produce CO. During the water splitting step, plasma dissociates H₂O into OH, O and H radicals providing a higher than normal O₂ fugacity [55], or P(O₂), over the CL material, leading to its more complete oxidation. The H radicals can combine to H₂ after losing the O atom to the CL material.

2. Experimental

2.1. Catalyst preparation and structural characterization

The nickel based perovskite catalyst (La_{0.9}Ce_{0.1}NiO₃) was prepared in a three step sol-gel [56–58] process. Ni(NO₃)₂·6H₂O (99.9985%, Alfa Aesar), La(NO₃)₃·6H₂O (99.90%, Alfa Aesar), and Ce(NO₃)₃·6H₂O (99.50%, Alfa Aesar) were used to prepare nitrate precursor solutions. The nitrate salts of the perovskite catalyst are mixed together in the proper ratios with distilled water to create an aqueous solution. Citric acid (99.0%, Alfa Aesar) and ethylene glycol (> 99.5%, TCI) are also added into the solution as complexing agents. The solution in a glass beaker was placed on a heated hotplate and with a magnetic stirrer, until all the water was evaporated. The dry precipitate was then hand ground using agate mortar and pestle and calcined at a temperature of 300 °C for 5 h in the box furnace. The perovskite powder was then removed and hand ground using agate mortar and pestle, after which it was calcined for a second cycle at 600 °C for 3 h. After the preparation of La_{0.9}Ce_{0.1}NiO₃ perovskite powder (50 nm), it was then combined with 100 nm size CeO₂ powder (99.99%, Alfa Aesar Reacton) in a 50:50 mass ratio. This mixture was then sintered at 1000 °C for 30 min and was hand ground for 10 min using agate mortar and pestle. A total mass of 200 mg was used in all the CL experiments.

The X-ray Diffraction (XRD) structural analysis of the as-prepared powder (La_{0.9}Ce_{0.1}NiO₃ + CeO₂ (LCN91Ce)) and the powders after high temperature and plasma treatments was executed in a Philips X'Pert MPD diffractometer. The diffraction patterns were recorded using Cu Kα source (λ = 0.154 nm) in the range of 2θ between 10° and 90° with a step size of 0.05°/min. The particle size and elemental mapping of the powders were characterized by scanning electron microscope (SEM; JEOL 7000 FE) coupled with an Energy Dispersive X-ray Spectrometer (EDS). N₂ physisorption at ~77 K (liquid nitrogen temperature) was used to determine the single point BET surface area of the sample in a Micromeritics AutoChem II 2920 chemisorption analyzer. The CL materials were characterized by SEM/XRD before and

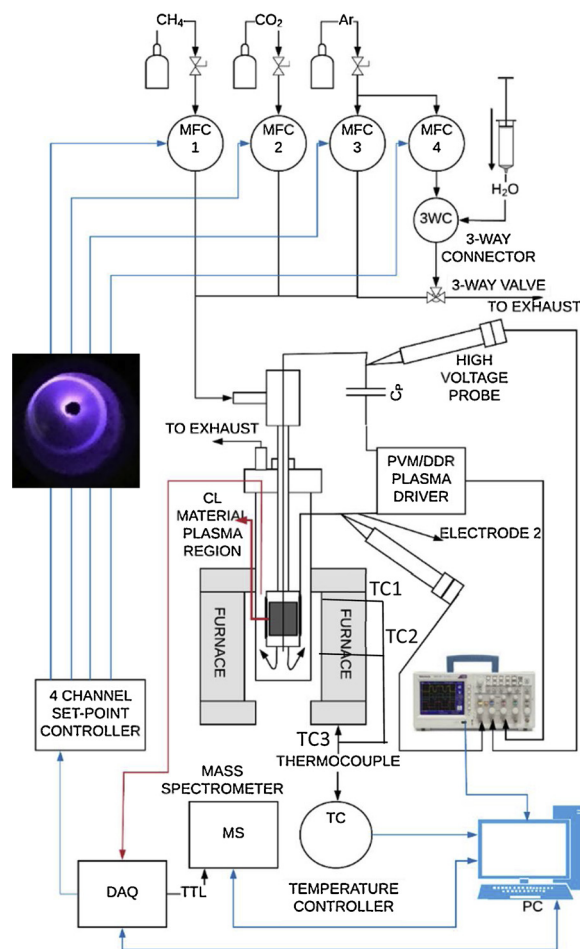


Fig. 3. Schematic of the CL test station setup. A bottom view picture of the plasma is shown on the left. TTL- Transistor to transistor logic, MS- Mass Spectrometer, TC1, TC2, TC3- Thermocouple, TC- Temperature Controller, PVM-DDR- Plasma Driver Brand used and DAQ- Data Acquisition system (Colors seen in the online version only, figure to be in single column).

after redox reactions.

2.2. Reactor setup

The CL test station consists of four parts – a gas delivery system, a central quartz reactor tube, experimental control section, and a flue gas analysis system. The design is based on that of Tianjiao Chen [58], modified for plasma discharge. The system layout and details of the reactor are shown in Fig. 3. The gas delivery system consists of four Brooks GF040 Multiflow thermal mass flow controllers (MFC), with < 1 s response times, which are controlled by a computer interface with a NI card. The NI card is controlled using a home written MATLAB GUI code. Gases with purity > 99.99% from Airgas, such as Ar, CH₄, CO₂, O₂ flow through these MFCs. A mixture of CH₄ and CO₂ was flowed during the reduction step. Pure Ar was flowed during the purging step. The water splitting oxidation step involves H₂O vapor and Ar mixture flow. Liquid water can be injected into the heated Ar flow line, using an automated syringe pump from New Era Pump Systems, which vaporizes as it enters the reactor for the oxidation step. Automated solenoid valves control the flow directions and redox phases.

The reactor consists of two concentric quartz tubes, which are placed inside an ATS 3210 split tube furnace. The furnace can heat up to 1100 °C and provides an isothermal environment. As shown in Fig. 3, three thermocouples are used to measure the temperature before and after experiments with plasma. The reactive gases are flowed into the

inner tube first which exits at the open end inside the outer tube, reverses direction and flows out to the exhaust. The inner quartz tube is of ¼" outer diameter (OD) with an expansion section of 3/8" inner diameter (ID) and 2" length. The reactive CL material, dispersed in quartz wool, is placed inside the expansion section of the inner quartz tube, directly in the plasma as will be explained below. The outside tube is of 1" OD and closed at one end.

A tiny capillary quartz probe (0.80 mm OD, 0.53 mm ID), is used to sample the gases and measure time resolved species at the probe end location, at the exit of the inlet tube expansion section where the CL material is placed in plasma. To analyze the gas composition a quadrupole mass spectrometer (QMS, model: MAX300-EGA from Extrel, 300 ms, 1-250 amu detectability), is used. The QMS is calibrated by flowing known mixture of gases. Signals at $m/e = 40, 44, 32, 2, 15, 18, 28$ are used to measure Ar, CO₂, O₂, H₂, CH₄, H₂O, and CO. CO₂ interferes with CO signals at 28 and its signals at 14 and 44 are used to correct the signals at 28 for CO. This is done by measuring fragmentation of CO₂ in the calibration process. The QMS calibration showed measurements to be accurate within $\pm 0.5\%$. All gases (H₂O, CO₂, CO, H₂, CH₄, Ar, O₂) were flowed simultaneously for calibration. The calibration was done at the beginning of the experiments. Calibration was tested every measurement before experiments, and if required, calibration was done again. We did not need re-calibration throughout these experiments completed within a week.

The flow conditions affecting gas residence time and the QMS sensitivity measurements were studied before the experiments. More details of similar analysis can be found in [3,5]. With increasing gas flow velocity, the gas residence time in the CL region decreases while the QMS sensitivity to species measurements decreased due to large dilution of H₂ by the balance gas, Ar in our case. A lower flow rate increases gas residence time and makes it comparable to reaction time constants (5–10 s) seen in our experiments. Therefore an optimum total volume flow rate of 350 sccm was chosen for our experiments. With this flow condition, the gas residence time at the CL material region is < 0.5 s. This is calculated by dividing the CL region volume by the gas volume flow rate at the reactor temperature. This enables quasi-steady approximations [50] for Plug Flow Reactor (PFR) heterogeneous reaction numerical modeling purposes, which will be the focus of our future studies.

The plasma generation setup contains two coaxial electrodes: one at the center of the inner inlet tube inside a 0.063 ID ceramic tube and the other on the outside of the expansion section of the inner inlet tube, giving rise to Dielectric Barrier Discharge (DBD) which produces non-equilibrium plasma. One of the electrodes is connected to the 20–70 kHz discharge PVM/DDR plasma driver power supply (from Amazing1.com) while the other electrode connected via a 1 nF capacitor (C_p) to the driver. The voltages are measured using two High Voltage Probes (HVPs) connected to the wires connecting the electrode to the plasma driver. The voltages on the HVPs are measured on an oscilloscope and processed to draw Lissajous curves to find the plasma power input by the method of Marcin Holub [59]. Fig. S1 (Supplementary file) shows the typical Lissajous curve obtained during the oxidation step. Here, the discharge voltage is plotted against the capacitor voltage. The power is calculated using a variation of Manley's approach using the formula:

$$P = f \cdot E = f \cdot \oint U_T \frac{dQ}{dt} dt = f \cdot C_p \oint U(t) dU_p \quad (1)$$

Here C_p is an additional capacitor used for measurement whose value is 1 nF in our experiments. $U(t)$ is the discharge voltage, U_p is the capacitor voltage, and f is the frequency of plasma discharge which is 20 kHz. The area in the loops of Fig. S1 is proportional to the plasma power supply. The measured average power during the redox cycles was in the range of 2–6 W for all temperatures. Plasma power temporarily varied during both the reduction and oxidation steps including the flow transition regime, and was different for different gas flows,

depending on the gas breakdown voltages [46]. However it was within 2–6 W. These measurements compare well with that of Yabe et al. [60] who obtained about 2.1–3.7 W for various metal doped Ni/M-ZrO₂ experiments. Most of the plasma power input is used to heat up the electric cables, electrodes etc., and less than 1% of the power supply is used in forming the plasma radicals and species [61]. Theoretically [61], up to 25% of the electric discharge power could be used in gas heating. A rough calculation for 350 sccm air flow, shows an increase in average gas temperature by 125 K. Nozaki et al. [61] experimentally found that less than 15% of electric discharge power was used for gas heating, and the average gas temperature increased by only 20–30 K for a plasma power supply similar to ours. The plasma is kept on during the continuous chemical looping experiments while furnace temperature is maintained at a constant level.

The measured concentrations of species are plotted as a function of time and used to study the reactions. The total flow rate of gases was maintained at 350 sccm (Standard Cubic Centimeter/min) during the redox cycles. The average velocity of the gas is ~ 6.48 cm/s at 298 K at the CL region. The flow during the reduction step is a mixture of CH₄ (100 sccm or 28.6 vol.%) and CO₂ (250 sccm or 71.4 vol.%). Ar (350 sccm) is used as purge gas. The flow during the oxidation step consists of argon and water vapor (2–10% H₂O with Ar). All experiments were conducted at 1 atm pressure, and in the temperature range of 150–1000 °C.

A single periodic CL cycle consists of a reduction step for 3 min followed by a purge step for 3 min and then an oxidation step for 1 min followed by a purge step for 3 min. Four different sets of experiments were conducted: (1) no CL material, no plasma; (2) no CL material, with plasma; (3) with CL material and no plasma; (4) with CL material and plasma. Experiments without plasma (case 3) were conducted by decreasing the reactor temperature from 1000 °C to 150 °C. Experiments with plasma and CL material (case 4) were conducted by first increasing the temperature (ramp up), and then, while decreasing the temperature (ramp down) in the same temperature range, to study the change in PC material behavior due to extreme temperature cycling. The furnace temperature was maintained constant for each redox cycle experiment.

2.3. Gas conversion analysis

To compare the performance with and without plasma during the reduction steps, the most important parameters are to quantify gaseous species conversion, selectivity, and yield [62]. The gas conversion (Eqs. (2) and (3)) is the ratio of the total amount of reactant consumed to the total amount of input reactant. The number of moles of reactant consumed is obtained by subtracting the number of moles of reactant measured from the number of moles of reactant input. The selectivity (Eqs. (4) and (5)) is defined as the ratio of desired product produced to the ratio of total reactant consumed. The yield of a reaction (Eqs. (6) and (7)) is defined as the ratio of the desired product produced to the total amount of reactant used. These terms are useful in identifying the consumption of the reactant, formation of the desired product and the selectivity towards a desired product. Carbon balance (Eq. (8)) is used to check for conservation in carbon atoms. The carbon deposition during reduction step is seen as CO₂ evolution during the oxidation step and is included in Eq. (8) for carbon balance analysis.

$$\text{CH}_4 \text{ Conversion } (X_{\text{CH}_4}) = \left[\frac{\text{Moles of CH}_4 \text{ consumed}}{\text{Moles of CH}_4 \text{ input}} \right] \times 100 (\%) \quad (2)$$

$$\text{CO}_2 \text{ Conversion } (X_{\text{CO}_2}) = \left[\frac{\text{Moles of CO}_2 \text{ consumed}}{\text{Moles of CO}_2 \text{ input}} \right] \times 100 (\%) \quad (3)$$

$$\text{CO Selectivity } (S_{\text{CO}}) = \left[\frac{\text{Moles of CO formed}}{\text{Moles of CH}_4 \text{ consumed} + \text{Moles of CO}_2 \text{ consumed}} \right] \times 100 (\%) \quad (4)$$

$$\text{H}_2 \text{ Selectivity } (S_{\text{H}_2}) = \left[\frac{\text{Moles of H}_2 \text{ formed}}{2 \times \text{Moles of CH}_4 \text{ consumed}} \right] \times 100 (\%) \quad (5)$$

$$\text{CO Yield } (Y_{\text{CO}}) = \left[\frac{\text{Moles of CO formed}}{\text{Moles of CH}_4 \text{ input} + \text{Moles of CO}_2 \text{ input}} \right] \times 100 (\%) \quad (6)$$

$$\text{H}_2 \text{ Yield } (Y_{\text{H}_2}) = \left[\frac{\text{Moles of H}_2 \text{ formed}}{2 \times \text{Moles of CH}_4 \text{ input}} \right] \times 100 (\%) \quad (7)$$

Carbon Balance

$$= \left[\frac{\text{Sum of Moles of CO, CO}_2 \text{ and CH}_4 \text{ formed (reduction)} + \text{Moles of CO}_2 \text{ formed (oxidation step)}}{\text{Moles of CH}_4 \text{ input} + \text{Moles of CO}_2 \text{ input}} \right] \times 100 (\%) \quad (8)$$

The total production or consumption of a species in a particular step in a redox cycle is calculated by time integrating the flow rate over the step time. For example, the total integrated H₂ produced (moles/g) during a reduction step required in Eq. (5) is calculated using

$$n_{\text{H}_2} = \frac{\int_0^t \dot{n}_{\text{H}_2} dt}{m_{\text{cat}}} = \frac{\left(\int_0^t x(t)_{\text{H}_2} \left(\frac{P\dot{V}}{RT} + \dot{n}_{\text{H}_2\text{O}} \right) dt \right)}{m_{\text{cat}}} \quad (9)$$

where, \dot{n}_{H_2} is the molar flow rate of H₂ in moles/s, $(P\dot{V}/RT + \dot{n}_{\text{H}_2\text{O}})$ is the total molar flow rate of gases into the reactor, $x(t)_{\text{H}_2}$ is the temporal H₂ mole fraction measured by the QMS, \dot{V} is the volumetric flow rate of the inflow gases measured by the MFCs at atmospheric pressure, P (101325 Pa), and temperature, T (298 K), and m_{cat} is the mass of the catalyst used for the experiment. R is the universal gas constant (8.314 kJ/kmole/K). Ideal gas assumptions have been made in Eq. (9). $\dot{n}_{\text{H}_2\text{O}}$ is the molar flow rate of water injected into the reactor. This can be found from the volume flow rate (syringe pump) and density of water at room temperature.

3. Results and discussions

3.1. Reforming tests of the CL material

To begin with, the effectiveness of the CL material (La_{0.9} Ce_{0.1} NiO₃ perovskite + CeO₂) for CH₄ reforming was tested, by flowing CH₄ (100 sccm) + CO₂ (250 sccm) mixture over three different materials of same total mass (200 mg) without plasma: (1) 100% CeO₂; (2) 100% La_{0.9} Ce_{0.1} NiO₃; (3) 50:50 mass ratio La_{0.9} Ce_{0.1} NiO₃ perovskite + CeO₂. The exhaust gases were analyzed using QMS. For these reforming measurements, the gases (CH₄ + CO₂) were flown for a longer time (~10 min) for the reforming to reach a steady state when all the oxygen from OC was consumed, and the CL material was reduced to a maximum extent at the reactor flow conditions. The lattice oxygen ions do not get consumed after reaching a steady state, but may play a role in the heterogeneous chemistry. Our purpose was only to test the dry reforming performance of perovskite/CeO₂ blend. The final steady state species percentage of H₂ in the exhaust flow is shown in Fig. 4 in the temperature range of 550–1000 °C. Fig. S2 shows the percentage CO and CH₄ in the exhaust flow, during CH₄ reforming in the temperature range of 550–1000 °C.

It is found that the reforming capacity of case 3 (perovskite + CeO₂) is not much different from case 2 (100% perovskite) while there is negligible reforming for case 1 (pure CeO₂). This shows catalytic reforming synergy between the perovskite and CeO₂ possibly due to the

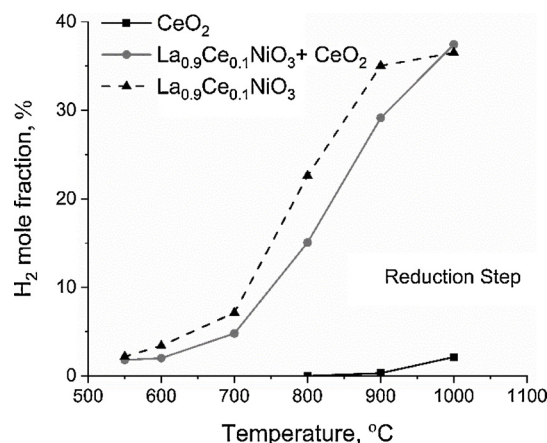


Fig. 4. % H₂ produced in the flow during steady state CH₄-CO₂ reforming. (Figure to be in one column).

shared high oxygen ion mobility characteristics and synergistic interface transfer chemistry, while achieving the higher oxygen carrying capacity with CeO₂ content in the mixture required for CL. CeO₂ can release lattice oxygen under oxygen lean conditions and store oxygen under oxygen rich conditions, mainly accommodated by a reversible valence change of cerium ions ($\text{Ce}^{4+} + e^- \leftrightarrow \text{Ce}^{3+}$ or $\text{O}^{2-} + 2\text{Ce}^{4+} \leftrightarrow 2\text{Ce}^{3+} + 1/2\text{O}_2(\text{g})$) with formation or elimination of oxygen vacancies. Therefore, case 3 material (perovskite + CeO₂) has been used for all CLRWS experiments that follow.

3.2. CLR with water splitting experiments-reduction step

Fig. 5 shows a typical redox cycle experimental data obtained at 1000 °C, measured using the Extrel QMS. Gases such as CO₂, CH₄, CO, H₂ and H₂O were detected during the reduction step. Gases such as H₂ and CO₂ were found during the oxidation step. A small spike of CO₂ was observed during the oxidation step the concentration of which increased with temperature. This spike is the result of carbon deposition during the reduction step. The measured temporal species profile can be time integrated to obtain the total species flowing in a step. For example, the H₂ profile can be integrated (similar to Eq. (8), shaded area in Fig. 5) to obtain the total moles of H₂ produced during the reduction step by CH₄ reforming. These integrated values were used for various types of analysis presented in Section 2.3.

We conducted three different experiments with CL material (a) CL

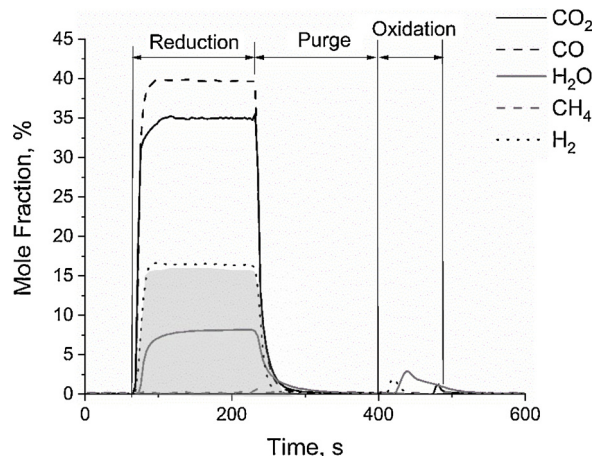


Fig. 5. Measured time resolved species mole fraction after flow over the CL material during a reduction/oxidation (redox) steps, at 1000 °C, 1 atm pressure. Reduction step: 3 min, Oxidation step: 1 min, and purge step: 3 min (Figure to be in one column).

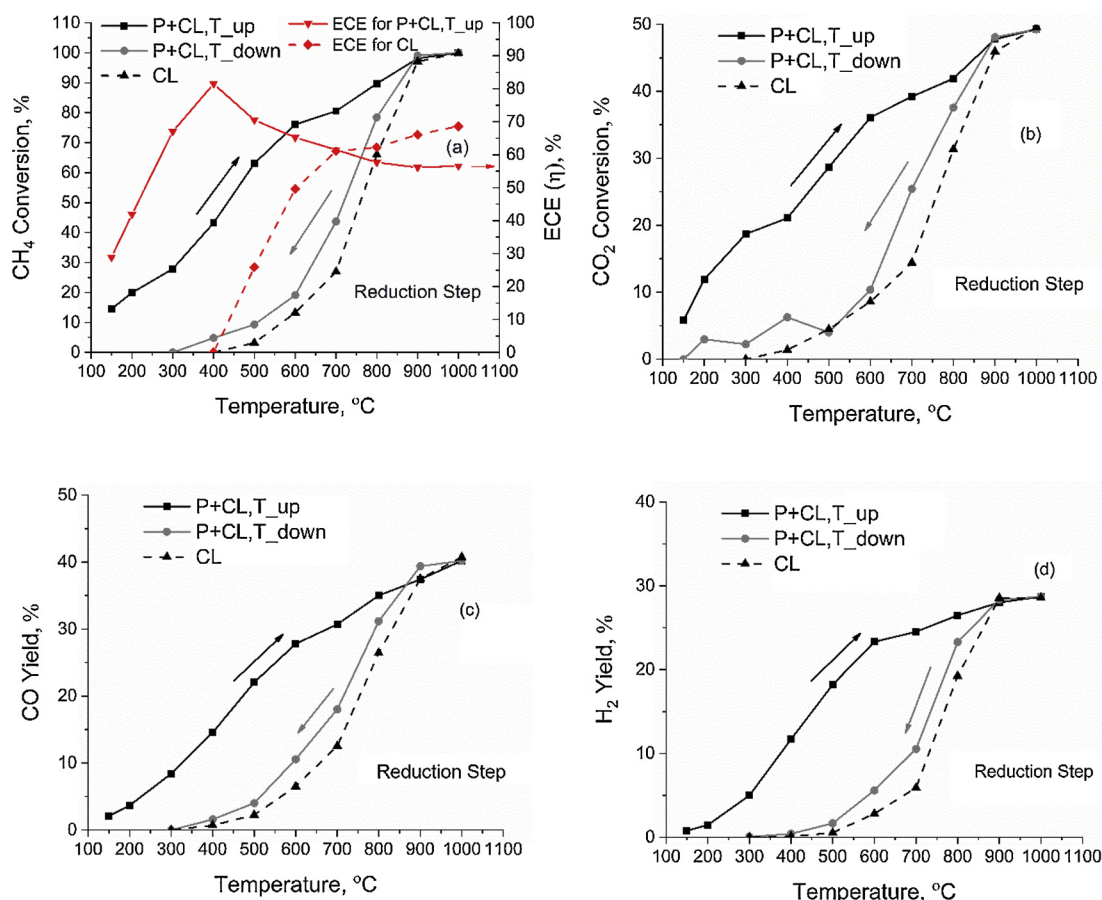


Fig. 6. (a) CH₄ Conversion & ECE (Energy Conversion Efficiency), (b) CO₂ Conversion, (c) CO Yield and (d) H₂ Yield at various temperatures, during reduction step. P: Plasma, CL: Chemical Looping material (Figure to be in two columns).

material is tested without plasma at different temperatures (indicated as CL in the figures); (b) CL material is tested with plasma at different temperatures with furnace temperature increased stepwise from 150 to 1000 °C (indicated as P + CL_T_up in the figures); (c) CL material is tested with plasma at different temperatures with furnace temperature reduced stepwise from 1000 to 150 °C (indicated as P + CL_T_down in the figures). The temporal molar flow rate of CO and H₂ at different temperatures with case (a), (b) and (c) is compared in Fig. S3. The integrated number of moles of various species such as CO and H₂ evolved during the reduction step at different temperatures are plotted in Fig. S4. Fig. 6 shows the integrated conversion of CH₄ and CO₂ and integrated yield of CO and H₂ by reforming for various temperatures. The moles of CH₄ and CO₂ indicated in Fig. S5 shows the integrated moles of CH₄ and CO₂ measured in the exhaust after consumption during reduction step vs. temperature. With the increase in temperature, the conversion increases resulting in less CH₄ and CO₂ measured in the exhaust as shown in Fig. S5. Fig. S6 shows the selectivity towards CO, H₂ formation vs. temperature by reforming.

The thermodynamic equilibrium calculation for the reactant mixture of CH₄ = 28.5% and CO₂ = 71.5% was done using CANTERA MATLAB [63] Equilibrium code and GRI mechanism [64] for the temperature range 100–1000 °C. The equilibrium concentrations of species such as CH₄, CO₂, CO, H₂O and H₂ are plotted vs. temperature in Fig. S7. Below ~ 400 °C, there is no formation of CO, H₂, and H₂O. Therefore, plasma enhances the low temperature reaction in our case. Experiments with ‘only plasma’ and ‘no CL material and no plasma’ showed insignificant reforming (< 1%) for temperatures below 900 °C, so results for these cases are not included in Fig. 6. At low temperatures (< 400 °C), yields are observed with case (b) when compared with case (a).

Increase in yields and conversions are observed with the increase in temperature for all three cases (Fig. 6). No reforming is observed in the temperature range 150–400 °C for case (a) and (c). However, there is a higher yield (62% enhancement at 600 °C) with plasma in case (c) compared to case (a) with no plasma. All three cases (Fig. 6) showed a CH₄ conversion of ~ 100% at 1000 °C and a CO₂ conversion of ~ 50% at 1000 °C. With temperature increasing up case (b), at 600 °C, the H₂ yield is 7.5 times and the CO yield is ~4.6 times that of case (a) with no plasma. The rate of increase in yield is higher from 150 to 600 °C for the case (b). CH₄ and CO₂ conversion of 14.7% and 5.78% respectively, is observed, at 150 °C with PC for the case (b). The decrease in yield for case (c) after cycling the CL material at 1000 °C can be assigned to the change in material structure, which will be discussed in Section 3.4. These PC results show substantial advantages for reactor construction and efficiency. For example, to achieve the same H₂ yields as at 500 °C with PC (case (b)), the reactor needs to be heated to 800 °C for the case without plasma (case (a)). Negligible change in CL material structure is expected below ~500 °C, leading to a more durable reactor.

In steady state PC reforming experiments, Yabe et al. [60] used Ni/La-ZrO₂, at 150 °C reactor temperature. With 3.7 W of applied power they reported 22.8% conversion of CH₄ and 24.8% conversion of CO₂ at an input flow rate of 100 sccm. These values are comparable to our CH₄ conversion values of ~15% at 150 °C and 350 sccm flow rates. PC Chemical looping combustion was performed by Zheng et al. [65], using a NiO/Fe₂O₃ catalyst at 400 °C. During the reduction step, a combination of CH₄ and Ar was flowed. Air was used for the oxidation step. A CH₄ conversion of 39% was achieved at 400 °C. These values are comparable to CH₄ reforming conversion of ~ 43% in our case.

Carbon inflow into the reactor is in the form of CH₄ and CO₂, while carbon outflow is in the form of CH₄, CO, CO₂. The difference between

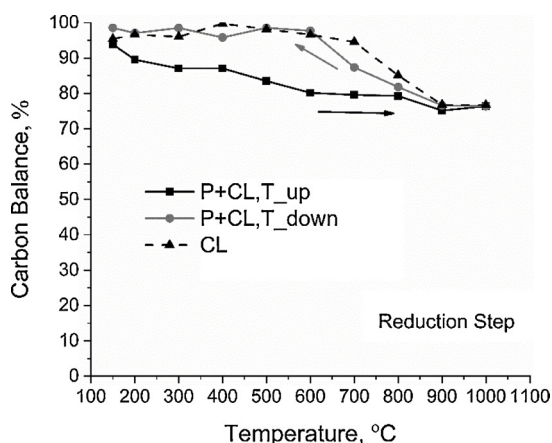


Fig. 7. Estimated carbon balance for the experiments at different temperatures. (Figure to be in one column).

time integrated carbon inflow and carbon outflow for one complete cycle (Eq. (7)) is shown in Fig. 7 for different temperatures. For experiments without plasma the carbon deficit is < 7% for temperatures < 700 °C, which then increases to ~ 20% at 1000 °C. For the PC case (increasing temperature experiments case), the carbon deficit gradually increased from 5% at 150 °C to ~24% at 1000 °C. Khoja et al. [62] also found similar carbon imbalance with plasma reforming. It is possibly because carbon was produced in other forms of C₂ hydrocarbon species such as C₂H₄, C₂H₆ and C₂H₂ by Oxidative Coupling of Methane (OCM) [66], in the initial phase of the reduction step when the CL material is being reduced, which were not measured in the current experiments. These species can also be formed in the gas phase plasma by the recombination of plasma radicals such as CH₃, CH₂, and CH on the catalyst surface or in the gas phase plasma. These undetected hydrocarbons may have contributed to the carbon balance deficit.

3.3. CLR with water splitting experiments-Oxidation step

Fig. 8 shows the temporal percentage H₂ flow measured using the QMS at the reactor exhaust, due to water splitting during the oxidation step for different temperatures. Fig. 9 shows the integrated H₂ produced by H₂O splitting at different temperatures for three different cases. No water splitting was observed below ~700 °C for case (a). For the case (b), we observed H₂O splitting at low temperatures (150–600 °C). For the case (c), PC performance of the CL material deteriorated after cycling the temperature at 1000 °C, with H₂O splitting observed only above 500 °C. Again this is attributed to CL material structural changes which will be explained in Section 3.4. The amount of H₂ production is limited by

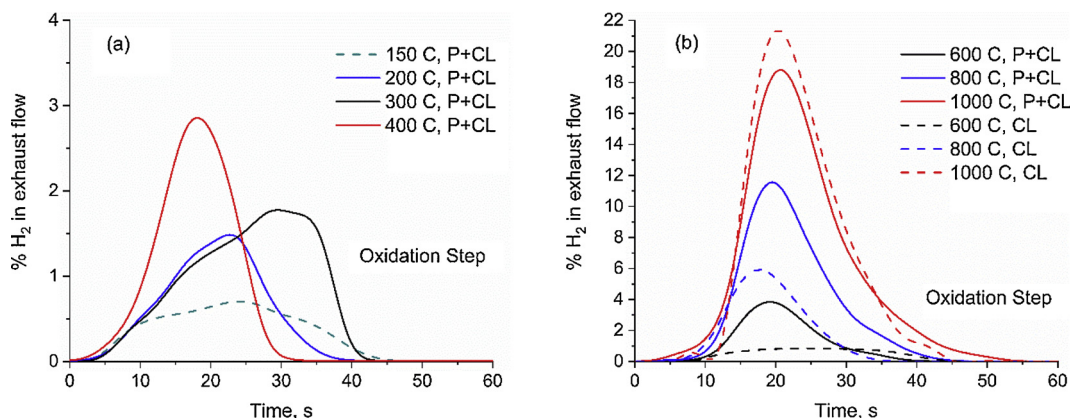


Fig. 8. Measured percentage H₂ flow in the exhaust in temperature range (a) 150–400 °C (b) 600–1000 °C. (Figure to be in one column, one below the other, color lines see only in the online version).

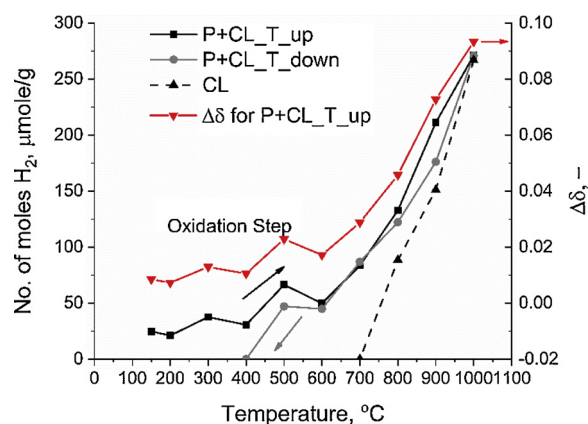


Fig. 9. Integrated H₂ production during as a function of temperature, with and without plasma. The change in performance during increase and decrease in temperature is also shown.

the oxygen carrying capacity of the OC and the extent of its reduction. More OC mass and higher level of reduction during the reduction step will give more H₂.

The higher amount of H₂ by water splitting with PC at all temperatures, is the outcome of greater extent of material reduction due to reactive plasma radicals produced during the reduction step such as the CH_x, H, CO by electron impact on CH₄ and CO₂. The oxidation of the CL material can be more complete with H₂O vapor in plasma due to abundant O atoms produced by electron impact dissociation of H₂O. Without the plasma, for H₂O/Ar flows, the fugacity of O₂ [55] is less than with O₂/Ar flows without the plasma. For example, it has been previously [3] found that water did not completely oxidize CeO₂ (without plasma) and another air flow step was required to completely oxidize CeO₂ at all temperatures. Time integrated number moles of CO + CO₂ flowed during oxidation step per integrated number of moles of CH₄ + CO₂ flowed during reduction step is plotted in Fig. S8. The numbers are within the range of 0.0002–0.0018. This means that there is less than 0.18% carbon deposition from the flow. There is a slight increase in carbon deposition with plasma catalysis.

The thermodynamic equilibrium calculations for the reactant mixture of H₂O = 10% and Ar = 90% was performed using CANTERA MATLAB [63] Equilibrium code from 1200 to 3000 °C. The equilibrium concentration of H₂ is plotted against temperature in Fig. S9. Below ~1500 °C, there is no formation of H₂. Atsushi Tsutsumi [67] did equilibrium calculations for pure H₂O and showed formation of H₂ only above temperatures of ~2000 °C. Therefore, we find that plasma catalysis is useful in enhancing H₂ production at very low temperatures.

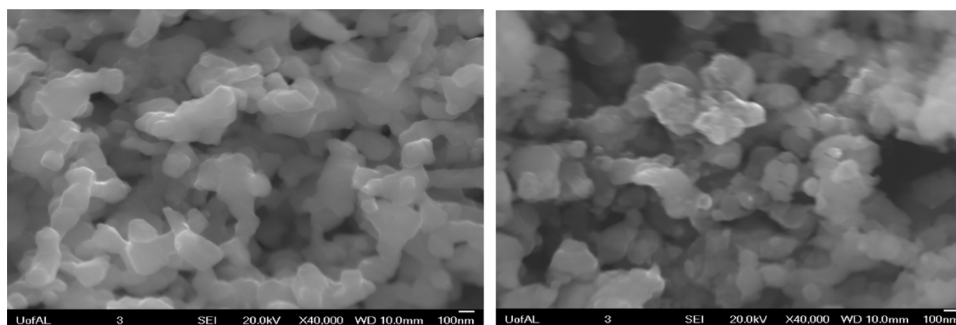


Fig. 10. LCN91Ce before (left) and after (right) experiment.

In Fig. 9 the calculated change in delta in CeO₂δ is shown for the oxidation step at different temperatures for the PC case with increasing temperature. This is calculated by dividing the total number of moles of hydrogen formed during the oxidation step by the total number of moles of ceria used in the experiment. The range of change in delta is 0.008–0.09. At 700 °C, the change in delta for the material ceria is 0.028. Zhao et al. [68] reported a non-stoichiometry increase of 0.03 at 700 °C and 0.20 at 1000 °C using water during the oxidation step while using H₂/Ar as fuel during the reduction step. After the oxidation step, the material was oxidized with 1% O₂ (balance Argon) and no further oxidation was found. Our lower values are possibly because of lesser extent of reduction due to the higher fugacity of O₂ in the CH₄/CO₂ flow compared to H₂/Ar flow [55].

3.4. CL material characterization

SEM images (Fig. 10) show the size of all particles to be in the range 100–200 nm, before and after redox cycling. No changes in particle size were observed after the CLR cycling up to 1000 °C for 50 cycles, as seen from the SEM images. The BET surface area of fresh La_{0.9}Ce_{0.1}Ni_{0.3}-CeO₂ sample was 10.54 m²/g.

The XRD patterns of the fresh CL materials, after 50 CLR cycles at 1000 °C and at 400 °C are shown in Fig. 11. The shown CL material cycled at 400 °C was not subjected to temperatures above 400 °C. Slight changes in the XRD patterns for the CL materials are seen, due to phase separation of Ni from the La_{0.9}Ce_{0.1}NiO₃ perovskite. There are signs of formation of oxides such as La₄Ni₃O₁₀ in fresh CL material. After experiments at 1000 °C, the same material changes to La₂O₃ and La₂NiO₄. The XRD patterns after 400 °C cycling showed very less differences in comparison to the fresh CL material. The EDS 2D mapping of the

materials (Fig. 12) also revealed slight separation of Ni as NiO. This may be the reason for the different PC behavior of the material during temperature ramp up and ramp down, as will be explained in the following sections. The change in material structure is expected to be lower for low temperature operation (150–500 °C).

3.5. Efficiency

Energy conversion efficiency (ECE) is reported by the Tao et al. [69] as a good indicator for understanding the efficiency of plasma reforming process. We calculated the ECE as the ratio of Lower Heating Value (LHV) of syngas produced in the reforming divided by the input power as in Eq. (10). It is desirable to have higher ECE.

$$ECE(\eta) = \frac{(\dot{n}_{CO}LHV_{CO}\bar{M}_{CO} + \dot{n}_{H_2}LHV_{H_2}\bar{M}_{H_2})}{(\dot{n}_{CH_4,in}C_{CH_4}LHV_{CH_4}\bar{M}_{CH_4} + P_{plasma} + P_{react})} \quad (10)$$

\dot{n}_{CO} and \dot{n}_{H_2} are the molar outflow rates of CO and H₂, respectively, \bar{M}_{CO} , \bar{M}_{CH_4} and \bar{M}_{H_2} are the molar masses of CO, CH₄ and H₂, respectively, $\dot{n}_{CH_4,in}$ is the molar inflow rate of CH₄, C_{CH_4} is the measured steady state CH₄ conversion fraction. LHV_X is the LHV of species X, $P_{plasma} = 6W$, is the measured plasma input power, P_{react} is the power required to heat the gas to the reactor inlet temperature. ECE calculated for the PC case (b) with increasing temperature is shown in Fig. 6a. With the increase in temperature, the ECE reaches an optimum high of 81.5% at 400 °C. Similarly, the ECE was calculated for the case (a) with only CL material and no plasma power and shown in Fig. 6a. The ECE is in the range of 0–68.2 % from 500 to 1000 °C, with cross over between the two cases at ~700 °C. While Case (b) shows higher overall ECE (81.5% at 400 °C), case (a) leads to complete CH₄ conversion for temperatures > 900 °C without plasma with ~68.2% ECE.

4. Conclusions

Plasma-catalysis Ni-based Perovskite mixed with ceria powder was experimented for chemical looping reforming step coupled with water splitting step in the temperature range 150 °C to 1000 °C. Experiments were conducted with and without plasma, during temperature ramp up and ramp down. Without plasma, the redox reactions were observed for temperatures > 700 °C. However, with PC synergy substantial reactions and yield was observed in 150–400 °C temperature range. Enhancements in yield and reactivity were also observed above 400 °C for the temperature ramp up PC experiments (case (b)). The study showed significant CH₄ and CO₂ conversion at 150 °C and enhancements at higher temperatures during temperature ramp up (case (b)). H₂ production by water splitting was observed with PC in 150–400 °C temperature range during temperature ramp up (case (b)). The conversion and yield decreased during the temperature ramp down from 1000 °C (case (c)). This is due to slight change in material structure at high temperature as verified by SEM and XRD images. Observed PC synergy implies efficiency improvement and many reactor construction advantages from lab scale to real time applications. For example, for the

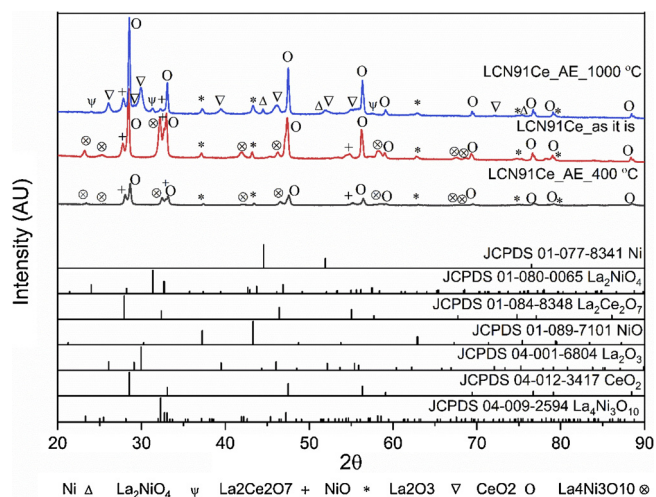


Fig. 11. XRD patterns of samples as it is and after experiments (AE) at 1000 °C and 400 °C.

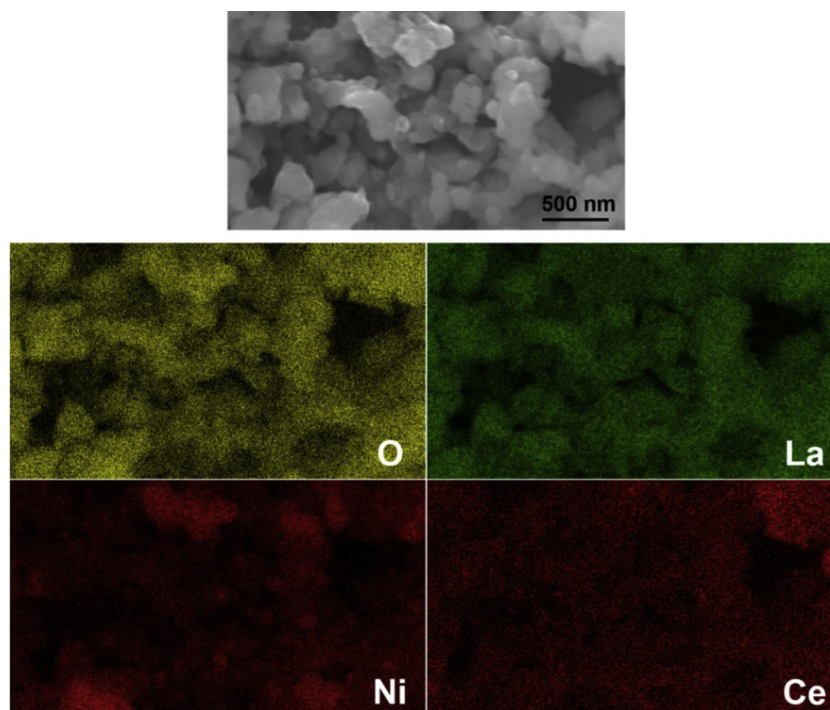


Fig. 12. SEM image and EDS elemental mapping analysis of LCN91Ce after experiment at 1000 °C (Colors seen in online version only, figure to be in one column).

same amount of H₂ production through PC water splitting at 300 °C would require ~ 750 °C without plasma. The required power to run the plasma in this temperature range is only 2–6 W. More efficient surface plasma discharges could be developed for real applications. The breakdown voltages of plasma are higher at higher pressures as defined by the Paschen curve. The breakdown is a function of both temperature and pressure, through the non-dimensional variable E/N , where E is electric field and N is concentration of neutral [70]. By applying high-pressure (in the range of 0.5–15 MPa) plasma hydrocarbon synthesis from syngas is reported in the literature [71]. We expect similar enhancement at higher pressures. We can achieve the required E/N values by modifying the surface plasma, plasma frequency, and peak voltages [36]. Thus, PC can enhance reactions at lower temperatures efficiently, while maintaining the integrity of materials over long hours. We find better advantages of PC at lower temperatures, reaching an optimum value at ~400 °C.

Many industries (power plants, oil companies etc.) have waste heat or renewable energy available in the temperature range 150–400 °C. The exhaust from power plants containing CO₂ can be used along with CH₄ to produce H₂ as demonstrated in this study. Although the conversion of CO₂ (14–43%) is not close to 100%, the authors think this is a considerable step towards usage of the CO₂. Examples of practical usage of such amounts of CO₂ conversion (14–43%) can be in stabilization of gas turbine combustion and development of solar-hybrid power plants [72]. The smaller amounts of syngas produced in our study at low temperatures can stabilize combustion, reduce NO_x emissions, improve efficiency and reduce acoustic noise in industrial burners [73,74] and gas turbines [75] while using lean mixtures of CH₄ mixed with syngas. Solar reactors can use feedstock CH₄ + CO₂ to generate chemicals such as H₂ which could be used for fuel cells. More advanced nano-materials for higher conversion of CH₄ + CO₂ to syngas will be the subject of future studies.

Acknowledgements

This work is supported by the NSF EPSCoR RII-Track-1 Cooperative Agreement OIA-1655280 and the first author was awarded a Graduate

Research Fellowship NSF EPSCoR. The authors also thank University of Alabama RGC (Research Grants Committee) grant for partial funding of supplies, Prof. Mark Weaver and Ms. Rachel White of Metallurgical and Materials Engineering Department, University of Alabama for help with the XRD experiments.

Appendix A. Supplementary data

Supplementary material related to this article can be found, in the online version, at doi:<https://doi.org/10.1016/j.jcou.2019.03.014>.

References

- [1] X.Y. Wu, L. Chang, M. Uddi, P. Kirchen, A.F. Ghoniem, Toward enhanced hydrogen generation from water using oxygen permeating LCF membranes, *Phys. Chem. Chem. Phys.* 17 (15) (2015) 10093–10107.
- [2] H.M. Kvamsdal, K. Jordal, O. Bolland, A quantitative comparison of gas turbine cycles with CO₂ capture, *Energy* 32 (1) (2007) 10–24.
- [3] Z. Zhao, Redox kinetics study for chemical-looping combustion and water splitting using nickel and cerium-based oxygen carrier, Mechanical Engineering, Massachusetts Institute of Technology, Cambridge, MA, USA, 2016.
- [4] M. Luo, Y. Yi, S. Wang, Z. Wang, M. Du, J. Pan, Q. Wang, Review of hydrogen production using chemical-looping technology, *Renew. Sustain. Energy Rev.* 81 (2018) 3186–3214.
- [5] Z. Zhao, M. Uddi, N. Tsvetkov, B. Yildiz, A.F. Ghoniem, Redox kinetics study of fuel reduced ceria for chemical-looping water splitting, *J. Phys. Chem. C* (2016) 16271–16289.
- [6] Z. Zhao, M. Uddi, N. Tsvetkov, B. Yildiz, A.F. Ghoniem, Redox kinetics study and non-stoichiometry characterization of Ce_{0.5}Zr_{0.5}O_{2-δ}, *J. Phys. Chem. C* 121 (21) (2016) 11055–11068.
- [7] Z. Zhao, M. Uddi, N. Tsvetkov, B. Yildiz, A.F. Ghoniem, Enhanced intermediate-temperature CO₂ splitting using nonstoichiometric ceria and ceria-zirconia, *J. Chem. Soc. Faraday Trans.* 19 (37) (2017) 25774–25785.
- [8] Z. Zhao, M. Uddi, N. Tsvetkov, B. Yildiz, A.F. Ghoniem, Redox kinetics and non-stoichiometry of Ce_{0.5}Zr_{0.5}O_{2-δ} for water splitting and hydrogen production, *J. Phys. Chem. C* 121 (21) (2017) 11055–11068.
- [9] Z. Zhao, M. Uddi, T. Chen, A.F. Ghoniem, Oxidation study for chemical-looping combustion using thin nickel foils, 9th U. S. National Combustion Meeting (2015).
- [10] D. Gielen, G. Symbolotti, Prospects for hydrogen and fuel cells, IEA Report, (2005).
- [11] M.V. Kathe, A. Empfield, J. Na, E. Blair, L.-S. Fan, Hydrogen production from natural gas using an iron-based chemical looping technology: thermodynamic simulations and process system analysis, *Appl. Energy* 165 (2016) 183–201.
- [12] (DOE), D.o.E. Department of Energy to Invest \$6.5 Million for Large-Scale Pilot Fossil Fuel Projects, (2018) Feb 15; Available from: <https://www.energy.gov/articles/department-energy-invest-65-million-large-scale-pilot-fossil-fuel-projects>.
- [13] Energy Department Invests \$12 Million in Coal Combustion Projects, (2017) Oct 20, 2017 Available from: <https://www.energy.gov/energy-department>.

- invests-12-million-coal-combustion-projects.
- [14] DOE Announces More Than \$10 Million for Advanced Combustion Systems Research, (2016) Sept 19, 2016.
- [15] J. Adánez, L.F. de Diego, F. García-Labiano, P. Gayán, A. Abad, J.M. Palacios, Selection of oxygen carriers for chemical-looping combustion, *Energy Fuels* 18 (2) (2004) 371–377.
- [16] K. Zhao, F. He, Z. Huang, G. Wei, A. Zheng, H. Li, Z. Zhao, Perovskite-type oxides LaFe_{1-x}CoxO₃ for chemical looping steam methane reforming to syngas and hydrogen co-production, *Appl. Energy* 168 (2016) 193–203.
- [17] T. Mattisson, M. Johansson, A. Lyngfelt, The use of NiO as an oxygen carrier in chemical-looping combustion, *Fuel* 85 (5) (2006) 736–747.
- [18] M. Johansson, T. Mattisson, A. Lyngfelt, A. Abad, Using continuous and pulse experiments to compare two promising nickel-based oxygen carriers for use in chemical-looping technologies, *Fuel* 87 (6) (2008) 988–1001.
- [19] P. Gayán, L. de Diego, F. García-Labiano, J. Adánez, A. Abad, C. Dueso, Effect of support on reactivity and selectivity of Ni-based oxygen carriers for chemical-looping combustion, *Fuel* 87 (2012) 2641–2650.
- [20] B. Abdullah, N.A.A. Ghani, D.-V.N. Vo, Recent advances in dry reforming of methane over Ni-based catalysts, *J. Clean. Prod.* (2017) 170–185.
- [21] L. Huang, F. Zhang, N. Wang, R. Chen, A.T. Hsu, Nickel-based perovskite catalysts with iron-doping via self-combustion for hydrogen production in auto-thermal reforming of ethanol, *Int. J. Hydrogen Energy* 37 (2) (2012) 1272–1279.
- [22] T. Hayakawa, S. Suzuki, J. Nakamura, T. Uchijima, S. Hamakawa, K. Suzuki, T. Shishido, K. Takehira, CO₂ reforming of CH₄ over Ni/perovskite catalysts prepared by solid phase crystallization method, *Appl. Catal. A Gen.* 183 (2) (1999) 273–285.
- [23] V.A. Sadykov, E.L. Gubanov, N.N. Sazonova, S.A. Pokrovskaya, N.A. Chumakova, N.V. Mezentseva, A.S. Bobin, R.V. Gulyaev, A.V. Ishchenko, T.A. Krieger, C. Mirodatos, Dry reforming of methane over Pt/PrCeZrO catalyst: kinetic and mechanistic features by transient studies and their modeling, *Catal. Today* 171 (1) (2011) 140–149.
- [24] S.M. Stagg-Williams, F.B. Noronha, G. Fendley, D.E. Resasco, CO₂ reforming of CH₄ over Pt/ZrO₂ catalysts promoted with La and Ce oxides, *J. Catal.* 194 (2) (2000) 240–249.
- [25] J. Chen, C. Yao, Y. Zhao, P. Jia, Synthesis gas production from dry reforming of methane over Ce_{0.75}Zr_{0.25}O₂-supported Ru catalysts, *Int. J. Hydrogen Energy* 35 (4) (2010) 1630–1642.
- [26] H.S. Whang, M.S. Choi, J. Lim, C. Kim, I. Heo, T.-S. Chang, H. Lee, Enhanced activity and durability of Ru catalyst dispersed on zirconia for dry reforming of methane, *Catal. Today* 293 (Suppl. C) (2017) 122–128.
- [27] D. Knapp, T. Ziegler, Methane dissociation on the ceria (111) surface, *J. Phys. Chem. C* 112 (44) (2008) 17311–17318.
- [28] P. Furler, J. Scheffe, D. Marxer, M. Gorbner, A. Bonk, U. Vogt, A. Steinfeld, Thermochemical CO₂ splitting via redox cycling of ceria reticulated foam structures with dual-scale porosities, *J. Chem. Soc. Faraday Trans. 16* (22) (2014) 10503–10511.
- [29] C. Ruan, Z.-Q. Huang, J. Lin, L. Li, X. Liu, M. Tian, C. Huang, C.-R. Chang, J. Jun Li, X. Wang, Synergy of the catalytic activation on Ni and the CeO₂-TiO₂-CeTi₂O₇ stoichiometric redox cycle for dramatically enhanced solar fuel production, *Energy Environ. Sci.* 12 (2019) 767–779.
- [30] S.J. Roberts, N.G. Carr, J. McLaughlin, H.E. Hagelin-Weaver, Iron precipitated onto ceria-zirconia nanoparticle mixtures for the production of hydrogen via two-step thermochemical water splitting, *Int. J. Hydrogen Energy* 43 (29) (2018) 12970–12984.
- [31] F.W. Sears, G.L. Salinger, *Thermodynamics, Kinetic Theory, and Statistical Thermodynamics*, 3rd. ed, Addison-Wesley, 1975.
- [32] K. Motzfeldt, *High Temperature Experiments in Chemistry and Materials Science*, John Wiley & Sons, Ltd, 2013.
- [33] W.C. Chueh, C. Falter, M. Abbott, D. Scipio, P. Furler, S.M. Haile, A. Steinfeld, High-flux solar-driven thermochemical dissociation of CO₂ and H₂O using nonstoichiometric ceria, *Science* 330 (6012) (2010) 1797–1801.
- [34] Z. Zhao, T. Chen, A.F. Ghoniem, Rotary bed reactor for chemical-looping combustion with carbon capture. Part 1: reactor design and model development, *Energy Fuels* 27 (1) (2013) 327–343.
- [35] M. Roeb, M. Neises, N. Monnerie, F. Call, H. Simon, C. Sattler, M. Schmücker, R. Pitz-Paal, Materials-related aspects of thermochemical water and carbon dioxide splitting: a review, *Materials* 5 (11) (2012) 2015.
- [36] M. Uddi, N. Jiang, E. Mintuossov, I.V. Adamovich, W. Lempert, Atomic oxygen measurements in air and air/fuel nanosecond pulse discharges by two photon laser induced fluorescence, *Proceedings of the Combustion Institute* 32 (2009) 929–936.
- [37] P. Mehta, P. Barbour, F.A. Herrera, J. Kim, P. Rumbach, D.B. Go, J.C. Hicks, W.F. Schneider, Overcoming ammonia synthesis scaling relations with plasma-enabled catalysis, *Nat. Catal.* 1 (4) (2018) 269–275.
- [38] E.C. Neyts, Plasma-surface interactions in plasma catalysis, *Plasma Chem. Plasma Process.* 36 (1) (2016) 185–212.
- [39] J.C. Whitehead, Plasma-catalysis: the known knowns, the known unknowns and the unknown unknowns, *J. Phys. D Appl. Phys.* 49 (24) (2016) 243001.
- [40] Y. Ju, J.K. Lefkowitz, C.B. Reuter, S.H. Won, X. Yang, S. Yang, W. Sun, Z. Jiang, Q. Chen, Plasma assisted low temperature combustion, *Plasma Chem. Plasma Process.* 36 (1) (2016) 85–105.
- [41] K. Hyun-Ha, Nonthermal plasma processing for air-pollution control: a historical review, current issues, and future prospects, *Plasma Process. Polym.* 1 (2) (2004) 91–110.
- [42] H.-H. Kim, Y. Teramoto, A. Ogata, H. Takagi, T. Nanba, Plasma catalysis for environmental treatment and energy applications, *Plasma Chem. Plasma Process.* 36 (45) (2016).
- [43] E.C. Neyts, A. Bogaerts, Understanding plasma catalysis through modelling and simulation—a review, *J. Phys. D Appl. Phys.* 47 (22) (2014) 224010.
- [44] T. Kim, S. Jo, Y.-H. Song, D.H. Lee, Synergetic mechanism of methanol-steam reforming reaction in a catalytic reactor with electric discharges, *Appl. Energy* 113 (2014) 1692–1699.
- [45] J.C. Whitehead, Plasma catalysis: a solution for environmental problems, *Pure Appl. Chem.* (2010) 1329.
- [46] Y.P. Raizer, *Gas Discharge Physics*, Springer-Verlag, Berlin Heidelberg, 1991.
- [47] G.S. Gallego, J.G. Marín, C. Batiot-Dupeyrat, J. Barraut, F. Mondragón, Influence of Pr and Ce in dry methane reforming catalysts produced from La_{1-x}AXNiO_{3-δ} perovskites, *Appl. Catal. A Gen.* 369 (1–2) (2009) 97–103.
- [48] R. Wang, P.A. Crozier, R. Sharma, Structural transformation in Ceria nanoparticles during redox processes, *J. Phys. Chem. C* 113 (14) (2009) 5700–5704.
- [49] J. Li, Z. Liu, R. Wang, Support structure and reduction treatment effects on CO oxidation of SiO₂ nanospheres and CeO₂ nanorods supported ruthenium catalysts, *J. Colloid Interface Sci.* 531 (2018) 204–215.
- [50] C.K. Law, *Combustion Physics*, Cambridge University Press, 2006.
- [51] I. Choi, Z. Yin, I.V. Adamovich, W.R. Lempert, Hydroxyl radical kinetics in repetitively pulsed hydrogen-air nanosecond plasmas, *IEEE Trans. Plasma Sci.* 39 (12) (2011) 3288–3299.
- [52] R. Snoeckx, R. Aerts, X. Tu, A. Bogaerts, Plasma-based dry reforming: a computational study ranging from the nanoseconds to seconds time scale, *J. Phys. Chem. C* 117 (10) (2013) 4957–4970.
- [53] H.K. Delgado, L. Maier, S. Tischer, A. Zellner, H. Stotz, O. Deutschmann, Surface Reaction kinetics of steam- and CO₂-reforming as well as oxidation of methane over nickel-based catalysts, *Catalysts* 5 (2) (2015).
- [54] X. Du, D. Zhang, L. Shi, R. Gao, J. Zhang, Morphology dependence of catalytic properties of Ni/CeO₂ nanostructures for carbon dioxide reforming of methane, *J. Phys. Chem. C* 116 (18) (2012) 10009–10016.
- [55] G. Zhou, P.R. Shah, T. Kim, P. Fornasiero, R.J. Gorte, Oxidation entropies and enthalpies of ceria-zirconia solid solutions, *Catal. Today* 123 (1) (2007) 86–93.
- [56] B.C. Dave, S.B. Lockwood, Sol-gel method, in: B. Bhushan (Ed.), *Encyclopedia of Nanotechnology*, Springer Netherlands, Dordrecht, 2012, pp. 2459–2470.
- [57] K. Mahendraprabhu, P. Elumalai, Influence of citric acid on formation of Ni/NiO nanocomposite by sol-gel synthesis, *J. Solgel Sci. Technol.* 73 (2) (2015) 428–433.
- [58] T. Chen, Experimental characterization and chemical kinetic study of chemical looping combustion, *Mechanical Engineering*, MIT, Cambridge, 2013.
- [59] M. Holub, On the measurement of plasma power in atmospheric pressure DBD plasma reactors, *Int. J. Appl. Electromagn. Mech.* 39 (2012) 81–87.
- [60] T. Yabe, K. Mitarai, K. Oshima, S. Ogo, Y. Sekine, Low-temperature dry reforming of methane to produce syngas in an electric field over La-doped Ni/ZrO₂ catalysts, *Fuel Process. Technol.* 158 (2017) 96–103.
- [61] T. Nozaki, K. Okazaki, Non-thermal plasma catalysis of methane: principles, energy efficiency, and applications, *Catal. Today* 211 (2013) 29–38.
- [62] A.H. Khoja, M. Tahir, N.A.S. Amin, Dry reforming of methane using different dielectric materials and DBD plasma reactor configurations, *Energy Convers. Manage.* 144 (2017) 262–274.
- [63] David G. Goodwin, R.L.S. Harry K. Moffat, Bryan W. Weber, *Cantera: An Object-oriented Software Toolkit for Chemical Kinetics, Thermodynamics, and Transport Processes*, (2018), <https://doi.org/10.5281/zenodo.170284> Version 2.4.0. <https://www.cantera.org>.
- [64] Gregory P. Smith, D.M.G., Michael Frenklach, Nigel W. Moriarty, Boris Eiteneer, Mikhail Goldenberg, C. Thomas Bowman, Ronald K. Hanson, Soonho Song, William C. Gardiner Jr., Vitali V. Lissianski, and Zhiwei Qin http://www.me.berkeley.edu/gri_mech/.
- [65] Y. Zheng, R. Grant, W. Hu, E. Marek, S.A. Scott, H₂ production from partial oxidation of CH₄ by Fe₂O₃-supported Ni-based catalysts in a plasma-assisted packed bed reactor, *Proc. Combust. Inst.* 37(4) (2018, 5481–5488).
- [66] Z. Cheng, D.S. Baser, S.G. Nadgouda, L. Qin, J.-A. Fan, L.-S. Fan, C₂ selectivity enhancement in chemical looping oxidative coupling of methane over a Mg-Mn composite oxygen carrier by Li-doping-induced oxygen vacancies, *ACS Energy Lett.* 3 (7) (2018) 1730–1736.
- [67] A. Tsutsumi, Chapter 2 – thermodynamics of water-splitting, in: T. Ohta (Ed.), *Solar-Hydrogen Energy Systems*, Pergamon, 1979, pp. 25–33.
- [68] Z. Zhao, M. Uddi, N. Tsvetkov, B. Yildiz, A.F. Ghoniem, Redox kinetics study of fuel reduced ceria for chemical-looping water splitting, *J. Phys. Chem. C* 120 (30) (2016) 16271–16289.
- [69] X. Tao, M. Bai, X. Li, H. Long, S. Shang, Y. Yin, X. Dai, CH₄-CO₂ reforming by plasma – challenges and opportunities, *Prog. Energy Combust. Sci.* 37 (2) (2011) 113–124.
- [70] M.A. Lieberman, A.J. Lichtenberg, second edition, *Principles of Plasma Discharges and Materials Processing Vol. 30* (2003).
- [71] S. Iwarere, V. Rohani, D. Ramjugernath, F. Fabry, L. Fulcheri, Hydrocarbons synthesis from syngas by very high pressure plasma, *Chem. Eng. J.* 241 (2014) 1–8.
- [72] D. Olivenza-León, A. Medina, A. Calvo Hernández, Thermodynamic modeling of a hybrid solar gas-turbine power plant, *Energy Convers. Manage.* 93 (2015) 435–447.
- [73] S.K. Alavandi, A.K. Agrawal, Experimental study of combustion of hydrogen-syngas/methane fuel mixtures in a porous burner, *Int. J. Hydrogen Energy* 33 (4) (2008) 1407–1415.
- [74] F. Bouras, El Hadi, M. Attia, F. Khaldi, M. Si-Ameur, Control of methane flame properties by hydrogen fuel addition: application to power plant combustion chamber, *Int. J. Hydrogen Energy* 42 (13) (2017) 8932–8939.
- [75] R.W. Schefer, D.M. Wicksall, A.K. Agrawal, Combustion of hydrogen-enriched methane in a lean premixed swirl-stabilized burner, *Proc. Combust. Inst.* 29 (1) (2002) 843–851.